J. Fluid Mech. (2025), *vol*. 1004, A11, doi:10.1017/jfm.2024.1179

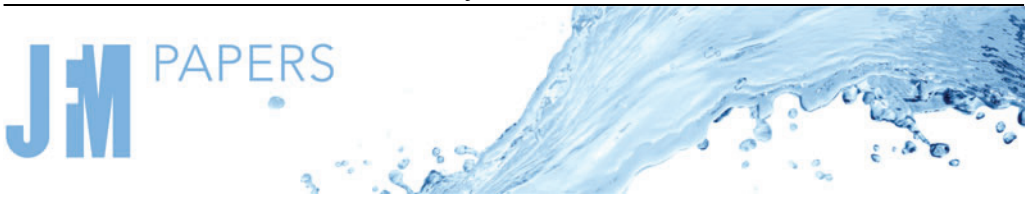

On the use of simplified geometries to represent turbulent flow over coral reefs

J.F. Hamilton[1],†, **B.Z. Kelley**[1], **S.G. Monismith**[1] **and J.R. Koseff**[1]

[1]Bob and Norma Street Environmental Fluid Mechanics Laboratory, Department of Civil and Environmental Engineering, Stanford University, Stanford, CA 94305, USA

(Received 25 October 2023; revised 14 October 2024; accepted 26 November 2024)

Hydrodynamic consequences of using simpler geometric shapes to represent coral canopies are examined through a laboratory study. A canopy composed of cylinders is compared with a canopy composed of 3-D-printed, scaled down coral heads in a recirculating flume. Vertical velocity profiles are measured at four horizontal locations for each canopy type, and mean velocity and turbulence statistics are compared both within and above the canopy. A narrow, defined wake on the scale of the canopy element is present behind the cylinder canopy elements that is absent in the coral canopy. There is also a peak in shear stress at the top of the cylinder canopy, likely due to the sharp edge at the top of the cylinder. Above the canopy, however, turbulence statistics and friction velocities behave similarly for both canopy types. Therefore, the results indicate we may reasonably get coral reef drag estimates from canopies with simpler geometric surrogates, especially when the mean free-stream and within-canopy flow speeds are matched to environmental conditions.

Key words: ocean processes, shear layer turbulence, turbulent boundary layers

1. Introduction

Despite occupying less than 1 % of the ocean floor, coral reefs are home to 25 % of all marine species (Hoegh-Guldberg *et al.* 2007). Unfortunately, 75 % of reefs are currently under threat from thermal impact events and subsequent bleaching (Burke *et al.* 2011). Coral functionality depends on ambient flow conditions, including turbulence-driven mixing, for nutrient and gas exchange (Atkinson & Bilger 1992). Accurately modelling flow in biogeochemical models of coral reefs is therefore key to better understanding how they will respond to environmental changes.

An inherent challenge in modelling coral reef systems is the broad range of spatial scales present, from kilometres to centimetres, contributing to the complexity of the flow

† Email address for correspondence: jhamil@stanford.edu

© The Author(s), 2025. Published by Cambridge University Press

https://doi.org/10.1017/jfm.2024.1179 Published online by Cambridge University Press

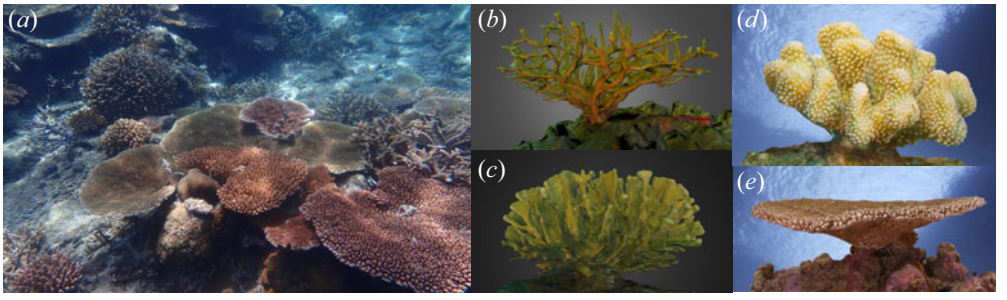

Figure 1. (*a*) Lighthouse reef in Palau. (*b*) *Acropora valenciennesi*. (*c*) *Pocillopora eydouxi*. (*d*) *Pocillopora meandrina*. (*e*) *Acropora hyacinthus*. Figure 1(*a*) sourced with permission from Alexy Khrizman; figures 1(*b*)–(*e*) reproduced with permission from The Hydrous at https://thehydro.us/3d-models.

(see figure 1*a*) (Rosman & Hench 2011). For instance, corals heads can extend for metres, their branches have diameters of just a few centimetres and individual polyps are no larger than a few millimetres (Wellington 1982). The phenomena affecting reef functioning occur at all of these scales (Madin & Connolly 2006; Hearn 2011; Rogers *et al.* 2018).

It is often not possible to keep the full scale of complexities when modelling coral reefs for predictive or exploratory purposes, so any modelled reef is a simplification. When modelling flows on the metre scale, it is common to represent the canopy using simple, replicable geometric shapes such as cylinders (Lowe, Koseff & Monismith 2005*a*; Lowe *et al.* 2005*b*; Madin 2005; Baldock *et al.* 2020) or wavy bedforms (Rogers *et al.* 2018). However, Stocking *et al.* (2018) showed that fine surface morphology details impact heat and mass transfer rates to and from the coral heads. Furthermore, studies of flow through densely packed coral skeletons show the effects of accurately representing in-canopy geometry on flow properties and dispersive stresses (Reidenbach, Koseff & Monismith 2007; Lowe *et al.* 2008; Asher *et al.* 2016; Asher & Shavit 2019; Pomeroy *et al.* 2023). Field observations by Hench & Rosman (2013) on a shallow backreef show reef-scale physical and biological processes are affected by flow patterns on the scale of coral patches. At an even finer scale (coral polyps), motile epidermal cilia enhance mass transport through ciliary beating (Shapiro *et al.* 2014), but these features are not typically represented in coral models. While the advantages of using simpler, reductionist geometries are clear, the impact of using a simplified coral structure on the hydrodynamics and heat and mass transfer in both models and experiments is not yet fully understood.

This study aims to investigate the hydrodynamic significance of one of these simplifications: using simple surrogates for coral heads on the flow in and around the canopy. Specifically, we examine (i) what important flow features are well captured by the simplified geometry, (ii) what important flow features are lost and (iii) are there any unintended consequences (e.g. introduction of flow features) when simplifying the complex coral roughness using simpler features. To address these questions, we experimentally compared flow characteristics over roughness composed of cylinders with flow characteristics over roughness composed of scaled coral replicates.

2. Methods

2.1. *Experimental facilities*

The experiments were conducted in an open-channel recirculating flume in the Bob and Norma Street Fluid Mechanics Laboratory at Stanford University. The flume's test section

https://doi.org/10.1017/jfm.2024.1179 Published online by Cambridge University Press

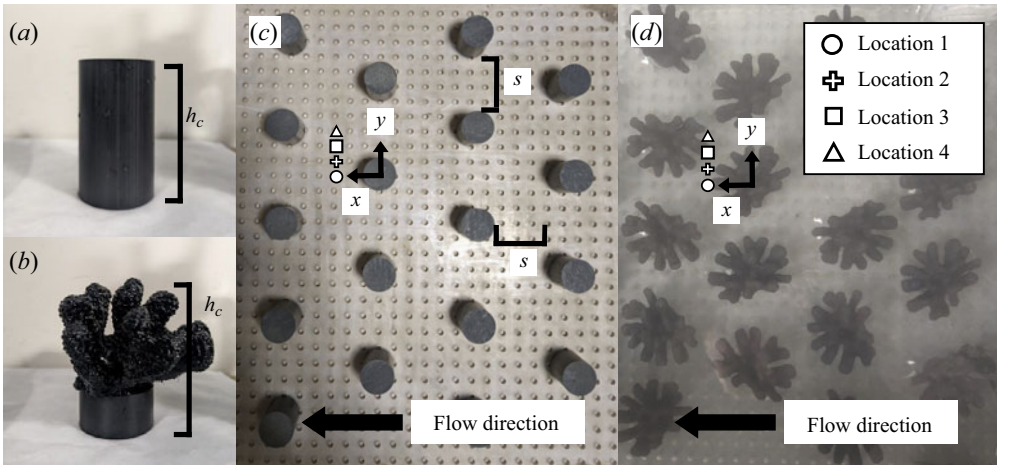

Figure 2. Canopy composition for (*a*) cylinders and (*b*) corals. Canopy element spacing and horizontal positions of velocity measurements are illustrated for (*c*) the cylinder canopy and (*d*) the coral canopy. Horizontal positions are evenly spaced ranging from directly behind the coral element (location 1) to in between two canopy elements (location 4).

measures 6 m long by 0.61 m wide. Flow is generated by a variable-speed pump filling a constant head tank. Water from the constant head tank passes through an inlet section consisting of a diffuser, homogenizing screens and a contraction before entering the test section, creating repeatable flow conditions. The canopies span the test section width, with the first and last 1.5 m of the flume canopy free to avoid effects from the inlet and outlet. Water levels were maintained at 32 cm. More details on the facility can be found in O'Riordan, Monismith & Koseff (1993).

2.2. *Canopy composition*

The coral canopy was modelled in two ways: first using cylindrical dowels (figure 2*a*) and second using scaled coral replicates (figure 2*b*). The scaled coral replicates were chosen to match common coral head characteristics: randomly oriented branches and non-uniform mass distributed with height. Many coral species have a cylindrical base with branches concentrated near the top of the canopy (figure 1*b–e*). To get the coral replicates, scans of living *Pocillopera meandrina* heads (figure 1*c*) were scaled down and then 3-D-printed to a height of 5 cm (three-dimensional models were provided open source by The Hydrous, https://thehydro.us/3d-models). The coral replicas were mounted on cylindrical bases cut from the same cylinders used for the cylinder canopy. Both the cylinder and 3-D-printed corals were 7 cm tall, giving a submergence ratio of $h_c/h = 0.22$, where h_c is the canopy height and h is the water depth. The spacing was kept consistent between canopy cases with $s = 8$ cm, $d = 4$ cm and $s/d = 2$ (figure 2*c*).

Ideally, volume, frontal area and canopy height would all be identical between the coral and the cylinder canopy cases. However, given that the 3-D-printed corals were made from scans of real corals, it was only possible to match one of the three physical characteristics when scaling down the coral model. Between volume, frontal area and canopy height, past research suggests it is most critical to match h_c/h between the two canopy cases (McDonald, Koseff & Monismith 2006). This choice resulted in the cylinders having 20 % less volume and 33 %–47 % smaller frontal area than the corals (depending on coral orientation). Thus, this study focuses on differences caused by shape complexity.

https://doi.org/10.1017/jfm.2024.1179 Published online by Cambridge University Press

While it is not appropriate to directly compare free-stream velocity, in-canopy velocity or the ratio between the two for each of the two canopies, it is appropriate to compare the shape of profiles (i.e. location of peaks) and relative differences between profiles in different locations (i.e. discussion of defined wakes).

2.3. *Velocity measurement system*

A 2-component laser-Doppler Anemometer (LDA) was used to measure instantaneous streamwise u and vertical w velocities. The entire LDA system was fixed to a platform with vertical and horizontal axis of motion. More details on the LDA system can be found in Mandel *et al.* (2017). Velocities were acquired at 14 heights above the bed: $z = [3.1, 3.9, 4.7, 5.5, 6.3, 8, 9.5, 11, 12.5, 15, 18, 21, 24, 27]$ cm, with $z = 0$ defined at the bed. We did not focus on capturing near-bed hydrodynamics in detail, as the primary goal of the experiment was to assess the overall flow similarities and differences behind and above the roughness elements. At each height, velocities were taken at four horizontal positions ranging from directly behind the canopy element to in between two canopy elements: $y/d = [0, 0.5, 1, 1.5]$ (figure 2*c*,*d*). Together, the instantaneous velocity profiles capture a representative range of the in-canopy and above-canopy dynamics. Measurement uncertainty comes from the following: vertical positioning of the LDA; the length of the time series; changes in water depth due to evaporation; the separation angle between the beams which affects estimates of u. The total measurement uncertainty is less than 5 % of the mean velocity.

2.4. *Data processing*

At each measurement location, a 10 minute time series of vertical and horizontal velocities was recorded at 200 Hz on average. The time series was despiked in a two-step process. First, all velocities above a non-physical threshold velocity were removed. The resulting time series was despiked using the phase-space method by Goring & Nikora (2002) modified by Mori, Suzuki & Kakuno (2007). After despiking, the time series was then filtered down to a uniform 50 Hz using a Gaussian filter function with 50 % overlapping windows.

Velocities were then decomposed into mean and fluctuating components. Overbars signify time averaging and ‘′’ signifies fluctuating components such that at any instant in time, $u = \bar{u} + u'$. Spectra were computed in four segments using a Hamming window with 50 % overlap.

3. Results

3.1. *Mean velocity profiles*

Streamwise flow for each canopy is shown in figure 3(*a*) for the cylinders and in figure 3(*b*) for the corals. Streamwise velocities are normalized by the free-stream velocity, which is 23 cm s^{-1} for the cylinder case and 24 cm s^{-1} for the coral case. To directly compare the two canopy cases, we plot the mean velocity profiles for the cylinders and corals together at location 1 (figure 3*c*) and location 4 (figure 3*d*). Figures 3(*c*) and 3(*d*) are normalized by the depth-averaged velocity, q/h, to keep the non-dimensionalization consistent between the two canopy cases. Here, q is the volumetric flow rate per unit width ($q = Q/b$ where b is the tank width) calculated by integrating the velocity profile from the bed to the free surface (assuming constant velocity over the top 5 cm in both cases).

https://doi.org/10.1017/jfm.2024.1179 Published online by Cambridge University Press

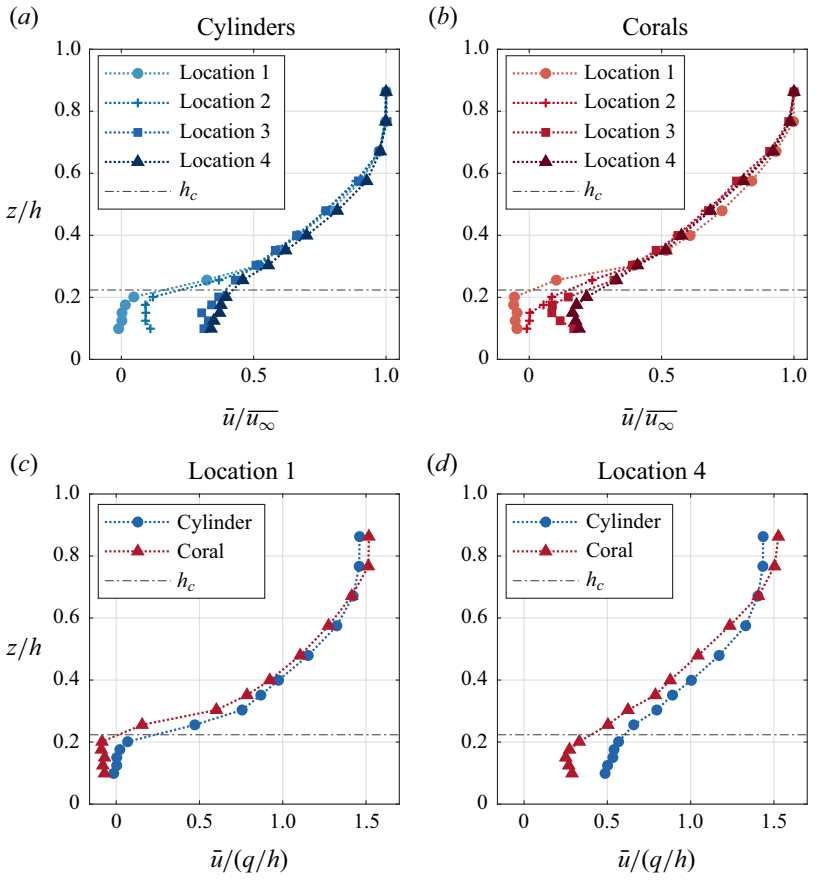

Figure 3. Mean streamwise velocities for (*a*) cylinders and (*b*) corals at all locations normalized by the free-stream velocity u_∞, and comparison of mean streamwise velocities at (*c*) location 1 and (*d*) location 4 normalized by the depth-averaged streamwise velocity q/h.

Some of the more notable similarities and differences in the profiles are as follows. First, the cylinder profiles show a well-defined, narrow wake within the canopy ($z/h < 0.22$) in the lee of the cylinders. This is illustrated by mean velocities less than 20 % of the free-stream velocity at locations 1 and 2 (inside the wake) compared with mean velocities greater than 40 % of the free-stream velocity at locations 3 and 4 (outside the wake). In contrast, the coral profiles show a broader wake. This observation is based on the less distinct difference between locations in the inner part of the wake (locations 1 and 2) and those on the outer portion of the wake (locations 3 and 4).

Second, the apparent wider influence of the corals (broader wake) seems to cause an overall slowdown of the flow within the canopy, with mean velocities at all locations less than 25 % of the free-stream velocity. In this experiment, the pump is set to maintain the same, constant flow rate for both experiments. Therefore, due to the increased resistance inside the coral canopy, there is a redistribution of velocity and consequently a greater fraction of the flow higher up in the water column (figure 3*b*,*c*). The differences in flow distribution between the in-canopy region and the free stream is due to a combination of the coral geometry and the larger coral frontal area, but it does not significantly impact overall drag due to a combination of factors that will be discussed in § 3.3.

https://doi.org/10.1017/jfm.2024.1179 Published online by Cambridge University Press

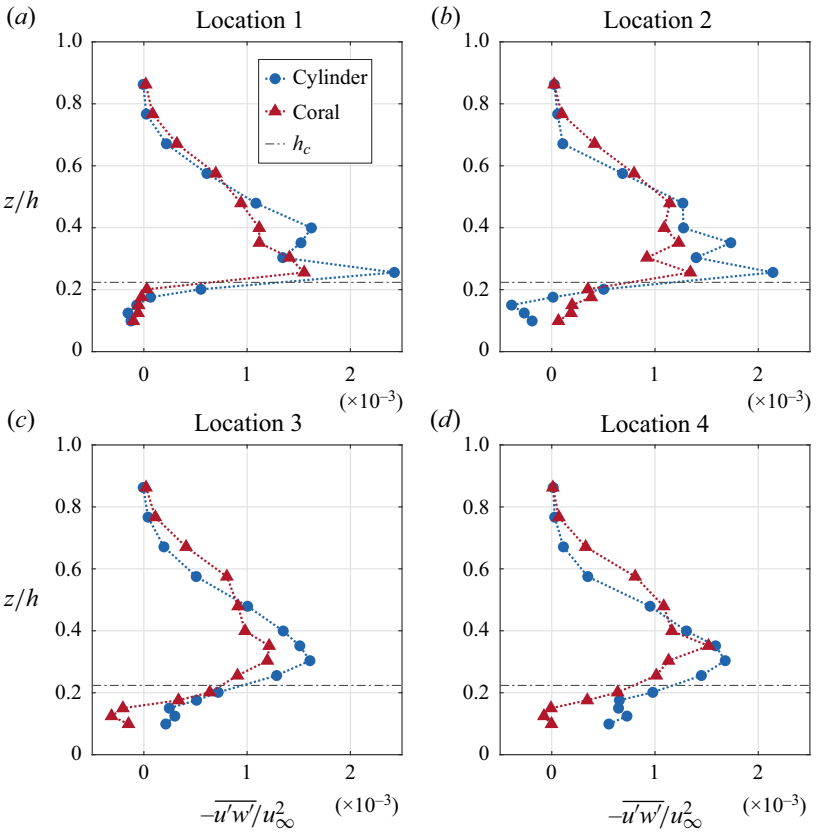

Figure 4. Comparison between coral and cylinder Reynolds stress profiles for all horizontal locations.

Third, our results indicate more recirculation within the coral canopy. In-canopy velocities at location 1 are in negative (reverse flow), averaging to approximately 10 % of the free-stream velocity. Furthermore, the corals have a local minimum velocity at the height of the branches which is absent in the cylinder velocity profiles.

3.2. *Turbulence characteristics*

In addition to differing mean flows within the canopy, turbulence statistics also vary between the two cases. Specifically, the in-canopy Reynolds stresses exhibit different behaviours between cases (figure 4). At all locations, but specifically wake locations 1 and 2, the cylinders have a higher peak Reynolds stress at the top of the canopy. This peak is likely caused by flow separation and vortex shedding off the cylinder's sharp top edge. At location 2, the stress increase above the canopy may stem from shear from both the top and the side of the cylinder. In contrast, the coral profiles lack the sharp peak observed in the cylinder case but have on average higher Reynolds stresses above the canopy ($z/h > 0.5$) at all locations, particularly locations 3 and 4. At location 4, higher in-canopy flow in the cylinder case leads to larger in-canopy stresses. The bootstrap uncertainties were at least an order of magnitude smaller than the Reynolds stress values and are too small to be discerned in figure 4.

Turbulent spectral density can also be used to evaluate similarities and differences between the two canopy cases. Coral and cylinder spectra are compared in wavenumber

https://doi.org/10.1017/jfm.2024.1179 Published online by Cambridge University Press

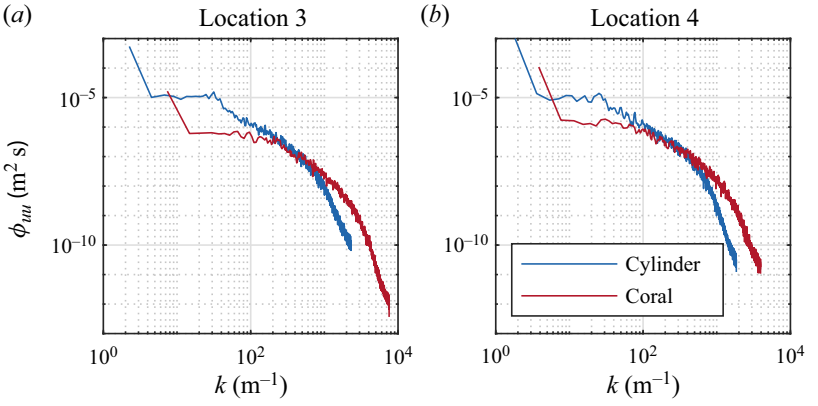

Figure 5. Comparison between coral and cylinder wavenumber spectra at $z/h = 0.15$ for horizontal location 3 and location 4, which is below the top of the canopy. The submergence ratio is 0.22.

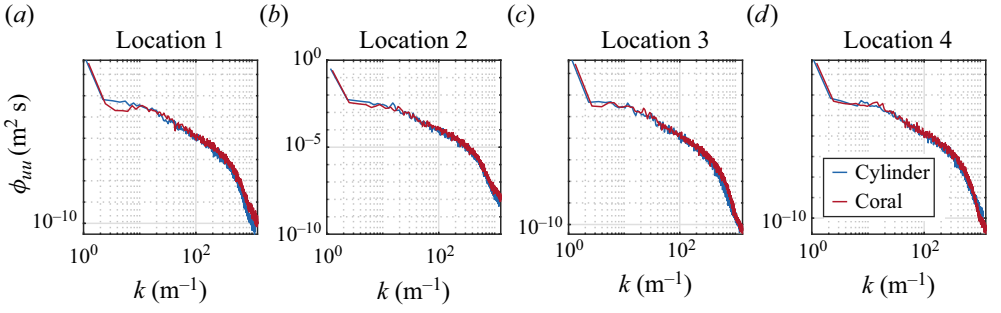

Figure 6. Comparison between coral and cylinder wavenumber spectra at $z/h = 0.35$ for all horizontal locations. The submergence ratio is 0.22.

space to remove differences caused by varying free-stream velocities. Taylor's frozen turbulence hypothesis is used to convert between frequency space and wavenumber space. However, the theory breaks down within the canopy at locations 1 and 2, as the time-averaged velocity is too slow for the assumption $\overline{u'^2}/\bar{u}^2 \ll 1$ to hold (Lin 1953). Therefore, only spectra at locations 3 and 4 are plotted. Figure 5 shows that, within the canopy, the coral spectra have more energy at higher wavenumbers (smaller scales), and less energy at lower wavenumbers (larger scales).

While in-canopy mean flows and turbulence statistics differ between cases, these differences become much less significant in the free stream (figure 6). Both canopies show similar rolloff behaviour and agree on all scales. To further examine how simplified corals affect the flow characteristics, we compared turbulent production profiles. In figure 7, production was calculated at each measurement height as

$$P = -\overline{u'w'}\frac{\mathrm{d}\bar{u}}{\mathrm{d}z} \tag{3.1}$$

(Pope 2012). Here, $\mathrm{d}\bar{u}/\mathrm{d}z$ was calculated by first fitting a cubic smoothing spline to the mean velocity profile by minimizing f in the equation

$$p\sum_{j=1}^{n}|\bar{u}_j - f(z_j)|^2 + (1-p)\int \lambda(t)|D^2 f(t)|^2\,\mathrm{d}t, \tag{3.2}$$

https://doi.org/10.1017/jfm.2024.1179 Published online by Cambridge University Press

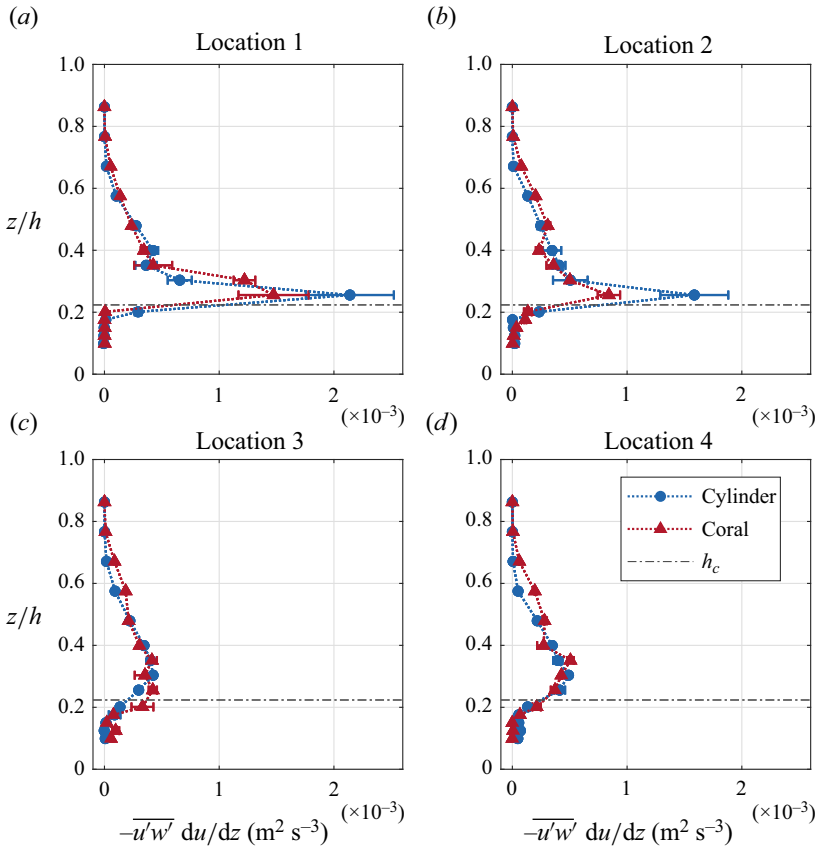

Figure 7. Comparison between coral and cylinder production profiles for all horizontal locations. Uncertainty comes from $\mathrm{d}u/\mathrm{d}z$ estimates.

where n is the number of measurement heights, $D^2f(t)$ is the second derivative of f and $\lambda = 1$ (de Boor 1980). The value of $\mathrm{d}\bar{u}/\mathrm{d}z$ was determined by evaluating the derivative of f at each measurement height. Uncertainty associated with $\mathrm{d}\bar{u}/\mathrm{d}z$ was calculated by adjusting the fitting parameter p in the range of $-4 * 10^{-7}$ to $+9 * 10^{-8}$. All values of p within this range gave acceptable spline fits.

Above the canopy, there were no significant differences in production at any location. Within the canopy there were small, location-dependent variations. At locations 1 and 2, the cylinders had 45–90 % greater peak production (at $z/h = 0.25$) than the corals due to the larger Reynolds stress from the cylinder's sharp top edge. However, these variations in production do not appear to be significant when considering the canopies' integrated drag. If the corals created significantly more drag than the cylinders, the pressure at the beginning of the canopy would be higher for the corals than the cylinders. Although pressure at the beginning of the canopy was not measured directly, upstream water levels were monitored. We observed no difference in water depth either before the canopy or at the end of the canopy between the two cases. Thus, the identical water levels and similar friction velocities (discussed in § 3.3) strongly suggest overall drag effects were the same.

To examine the potential differences in mass transfer rates caused by using a simpler cylinder surrogate for the coral heads, we used turbulent dissipation as an indicator of the mixing that brings nutrients and gasses to coral surfaces. Dissipation was determined by

https://doi.org/10.1017/jfm.2024.1179 Published online by Cambridge University Press

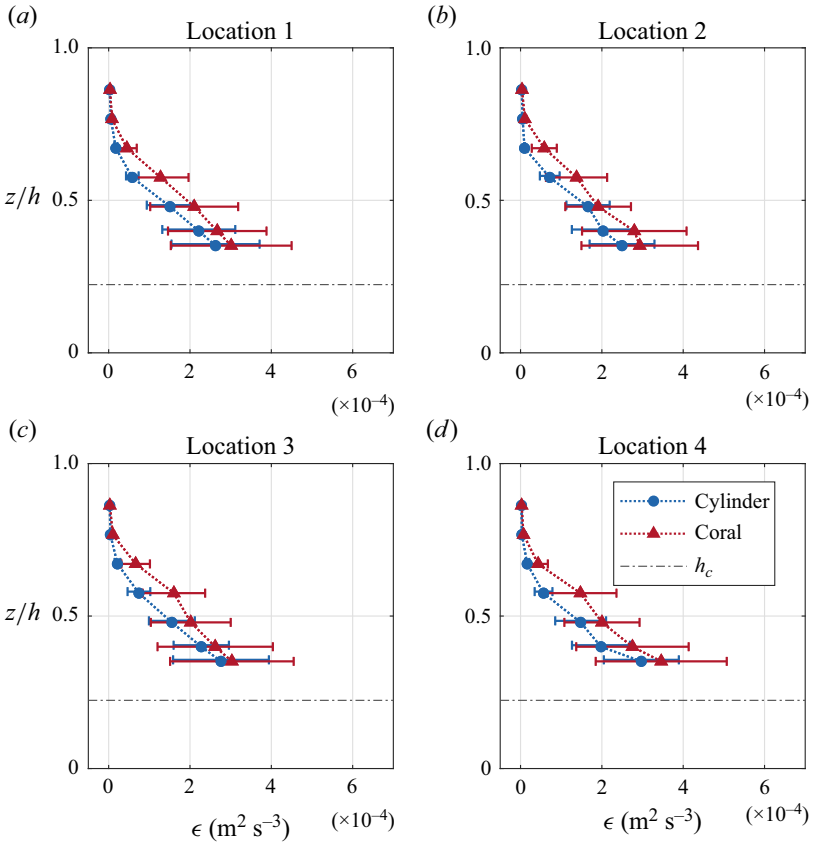

Figure 8. Comparison between coral and cylinder dissipation for all horizontal locations. Uncertainty comes from differences in ϵ due to which spectrum (ϕ_{uu} or ϕ_{ww}) ϵ is calculated from and the sensitivity to inertial subrange frequency bounds.

fitting $f^{-5/3}$ to the inertial subrange of the frequency spectra and then calculating ϵ as

$$\phi_{uu} = A\left(\frac{18}{55}\right)\epsilon^{2/3}\left(\frac{U}{2\pi}\right)^{2/3} f^{-5/3}, \quad \phi_{ww} = \frac{4}{3}\phi_{uu}, \tag{3.3a,b}$$

where $A = 1.5$ (Nepf & Vivoni 2000). Dissipation was only evaluated above the canopy due to the high turbulence intensity relative to the mean streamwise velocity inside the canopy (Lumley 1965). Figure 8 shows the dissipation profiles for each location. The uncertainty in our measurements comes, in part, from disagreement between dissipation calculated from the streamwise velocity spectra and dissipation calculated using the vertical velocity spectra, even with the 4/3 adjustment (3.3*a*,*b*). The maximum difference between dissipation calculated from ϕ_{uu} vs ϕ_{ww} occurred at the points closest to the top of the canopy. The frequency bounds of the inertial subrange $f^{-5/3}$ fit also contribute to uncertainty as there are multiple frequency bands where the linear regression of $f^{-5/3}$ is a good fit. Uncertainty associated with the $f^{-5/3}$ frequency band choice was quantified as the difference between ϵ calculated using the widest frequency range with a reasonable fit (6 hz) and ϵ calculated using the narrowest frequency range with a reasonable fit (3 hz). The uncertainty ranges associated with velocity spectrum choice and the uncertainty range

https://doi.org/10.1017/jfm.2024.1179 Published online by Cambridge University Press

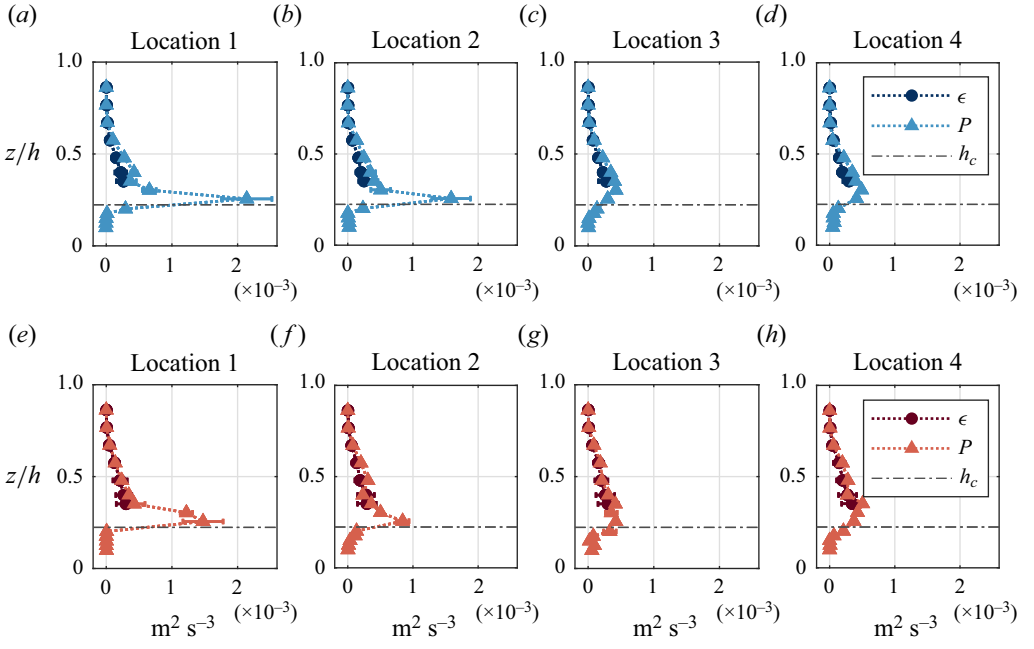

Figure 9. Comparison of spatially averaged production and dissipation profiles for each canopy type. Blue top row is the cylinder canopy case and red bottom row is the coral canopy case.

frequency band choice were calculated as

$$\delta\epsilon_d = \left| \frac{\epsilon_{3\text{ Hz},\phi_{uu}} + \epsilon_{6\text{ Hz},\phi_{uu}}}{2} - \frac{\epsilon_{3\text{ Hz},\phi_{ww}} + \epsilon_{6\text{ Hz},\phi_{ww}}}{2} \right|, \tag{3.4}$$

$$\delta\epsilon_f = \left| \frac{\epsilon_{3\text{ Hz},\phi_{uu}} + \epsilon_{3\text{ Hz},\phi_{ww}}}{2} - \frac{\epsilon_{6\text{ Hz},\phi_{uu}} + \epsilon_{6\text{ Hz},\phi_{ww}}}{2} \right|, \tag{3.5}$$

$$\delta\epsilon = \sqrt{\delta\epsilon_f^2 + \delta\epsilon_d^2}, \tag{3.6}$$

where $\epsilon_{3\text{ Hz},\phi_{uu}}$ is the dissipation calculated by fitting $f^{-5/3}$ to a 3 Hz frequency band in ϕ_{uu}, $\epsilon_{3\text{ Hz},\phi_{ww}}$ is the dissipation calculated by fitting $f^{-5/3}$ to a 3 Hz frequency band in ϕ_{ww}, $\epsilon_{6\text{ Hz},\phi_{uu}}$ is the dissipation calculated by fitting $f^{-5/3}$ to a 6 Hz frequency band in ϕ_{uu} and $\epsilon_{6\text{ Hz},\phi_{ww}}$ is the dissipation calculated by fitting $f^{-5/3}$ to a 6 Hz frequency band in ϕ_{ww}. Here, $\delta\epsilon_f$ is the uncertainty associated with frequency band choice, $\delta\epsilon_d$ is the uncertainty associated with differences in ϵ from using either ϕ_{uu} or ϕ_{ww} and $\delta\epsilon$ is the total uncertainty shown in figure 8.

At all locations, the dissipation peaks just above the canopy before decreasing with height. Although the coral canopy exhibits higher dissipation rates at all heights, the difference is within the uncertainty bounds. The close match of dissipation and production between the coral and cylinder cases, despite differences in frontal area, volume and mean velocity profiles within the canopy, indicates that precisely matching frontal area and volume has little impact on free-stream turbulence statistics.

Production and dissipation can be compared directly at each location to see if transport terms in the turbulent kinetic energy (TKE) equation significantly affect either canopy case (figure 9). As discussed above, dissipation was only plotted starting above the canopy, so further work is needed to examine transport terms within the canopy. There is good

https://doi.org/10.1017/jfm.2024.1179 Published online by Cambridge University Press

agreement in both canopy cases at heights where production and dissipation can be directly compared, with differences within uncertainty bounds, suggesting small TKE transport terms. The similarities between the corals and cylinders as shown in figures 8 and 7, therefore, strongly indicate that cylinders do an adequate job of capturing the overall structure of the boundary layer above a coral reef.

3.3. *Estimating drag*

The drag coefficient, C_D, is necessary for determining the drag term in the momentum equation. Here, C_D can be calculated as

$$C_D = u_*^2 / U_{ref}^2, \tag{3.7}$$

where u_* is the friction velocity and U_{ref} is a reference velocity defined in the field as either velocity at 1 m above the bed or the depth-averaged velocity (e.g. Reidenbach *et al.* 2006; Lentz *et al.* 2017). Given the highly resolved two-dimensional velocity profile, we are able to calculate u_* using three separate method in order to evaluate the effect of canopy element simplification on drag estimates. All three methods described below are commonly used interchangeably in the field to calculated drag coefficients (Takeshita *et al.* 2016).

Log-fitting method: the friction velocity can be derived from fitting the velocity profile to the log law (Pope 2012)

$$\bar{u}(z) = \frac{u_*}{\kappa} \ln\left(\frac{z-d}{z_0}\right), \tag{3.8}$$

where d is the displacement height and $\bar{u}(z)$ is the spatially averaged velocity profile. We begin log fitting at $2h_c$ to avoid accidentally fitting to the roughness sublayer which does not follow the log law (Brunet 2020). Because there are three fitting parameters (u_*, z_0 and d), values of d were chosen to range from $z = 0$ to $z = h_c$. All values of d show excellent agreement with $R^2 > 0.93$ (figure 10*a*,*c*).

Dissipation method: spectrally derived dissipation was used to calculate friction velocity as

$$u_* = (\epsilon \kappa z)^{1/3}, \tag{3.9}$$

where κ is the von Kármán constant and z is the height above the bed. The dissipation-derived u_* can only be calculated above the canopy (Lumley 1965).

Covariance method: the Reynolds stress at the bed can be related to the friction velocity (e.g. Lindhart *et al.* 2021) as

$$u_* = \overline{|u'w'|_b}^{1/2}. \tag{3.10}$$

Above the bed, the Reynolds stress is expected to decrease linearly with height, reaching zero at the surface. Therefore, a depth correction must be added when using measurements higher up in the water column. Additionally, in the presence of large roughness elements, the maximum Reynolds stress occurs at approximately h_c instead of at the bed, so friction velocity is calculated as

$$u_* = \overline{|u'w'|_z}^{1/2} * \left(1 - \frac{z-h_c}{h-h_c}\right)^{-1/2}. \tag{3.11}$$

For the dissipation and covariance methods, peak u_* occurs withing 1.5 canopy heights, and then decreases with proximity to the surface. The values of u_* for those two methods

https://doi.org/10.1017/jfm.2024.1179 Published online by Cambridge University Press

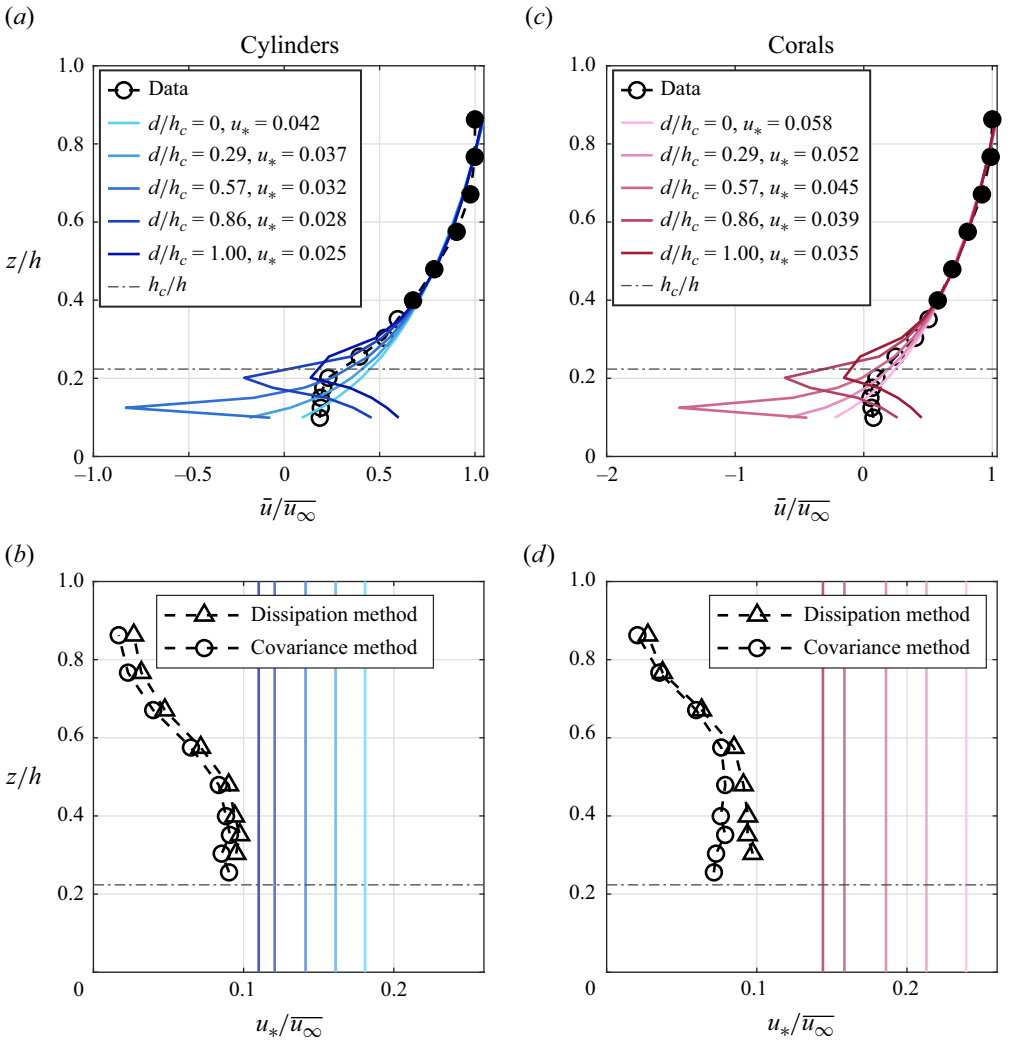

Figure 10. Log fits to spatially averaged velocity profile with various displacement heights (d) and the resulting u_* for (a) the cylinder canopy and (b) the coral canopy. The log law was fit to the filled circles only. Comparison of spatially averaged u_* values calculated using the dissipation, covariance, and log-law methods for (c) the cylinder canopy and (d) the coral canopy. Vertical lines are log fit u_* coloured by d/h_c.

largely agree both across canopy cases and between methods. The agreement between canopy cases is likely due to opposing mechanisms. For the cylinder canopy, the sharp edge leads to a peak in shear stress which increases overall drag. For the coral canopy case, the steeper velocity gradient causes more instabilities, but the slower in-canopy flow results in a higher U_{ref}. Overall, this implies that individual shape complexity does not significantly impact overall drag (figure 10*b*,*d*).

However, across all values of d/h_c, u_* calculated using the log-fitting method is consistently higher in the coral canopy case than the cylinder case. It is also up to 3 times greater than u_* calculated using dissipation and covariance methods, and very sensitive to displacement height choices (figure 10*a*,*c*). Typically, u_* derived from log fits represents an integrated drag that incorporates changes in topography and patchiness, which has been noted in field studies (Rosman & Hench 2011). This experimental set-up represents a

https://doi.org/10.1017/jfm.2024.1179 Published online by Cambridge University Press

uniform canopy with no changes in topography or patchiness, suggesting that the corals are behaving (collectively) as a full canopy instead of as individual large roughness elements and a log layer does not exist. We caution the use of log fits to calculate drag coefficients when the submergence ration h_c/h is of the order of 0.2 or greater, independent of canopy element complexity.

3.4. *Parameter space considerations*

This study is a detailed investigation of a relatively small parameter space. However, by carefully choosing the experimental parameters and using the results of related studies we can minimize the need for examining large parameter ranges. First, while varying the mean flow would produce a wider range of Reynolds numbers, once a flow is fully developed ($Re > 10^4$), the Reynolds number has only a small effect on the turbulence dynamics and mixing (Dimotakis 2000). Second, cylinder size and spacing were chosen to match the spacing set in Lowe *et al.* (2005*a*,*b*). Lowe *et al.* (2005*a*) showed that, as canopy spacing becomes denser ($S/d = 1$), the velocity inside the canopy decreases and the Reynolds stress increases. Both changes happen monotonically, suggesting a similarly monotonic change in the coral canopy as well. The differences in velocity and Reynolds stress are most significant within the canopy and only slightly affect the flow above the canopy, indicating that the above-canopy similarities between the corals and the cylinders will remain similar even with varied spacing.

Third, canopy flow depends on the submergence ratio h_c/h in that as submergence ratio increases, more flow is forced through the canopy (McDonald *et al.* 2006). In instances where canopy element simplification impacts results, we expect the impact to increase as submergence ratio increases. Finally, the coral canopy in this study consists of only one type of coral. Universally, corals have branches, smooth edges and bumpy surfaces (figure 1), so we chose a coral exhibiting all of these common features.

There are additional complexities not accounted for in this study. Since the experiment had unidirectional flume with uniformly distributed canopy elements, neither case captures the spatial and temporal complexities of living reefs, where coral coverage is typically heterogeneous and patchy. Furthermore, the 3-D-printed coral heads most closely resemble branching corals, and it has been shown that tabletop corals lead to a different ratio of in-canopy to free-stream flow (Pomeroy *et al.* 2023). Oscillatory flow also impacts both mass transfer (Lowe *et al.* 2005*b*) and larval dispersion (Reidenbach, Koseff & Koehl 2009; Reidenbach *et al.* 2021). Additional work needs to be done to apply these results to corals of varying geometries.

4. Conclusion

This work presents an experimental hydrodynamic comparison between a coral head canopy and a cylinder canopy allowing us to conclude the following. Cylinder canopies have defined, narrow wakes in the lee of the cylinders and higher stresses at the top of the canopy associated with the cylinder's sharp edges. In contrast, coral head canopies exhibit broader, more muted wakes. Additionally, the coral branches increase resistance within the canopy, consequently redistributing flow to higher up in the water column.

Despite these in-canopy differences and the introduction of additional shear at the top of the cylinder canopy, the turbulence statistics, mean velocities and friction velocities largely agree above the canopy. This indicates that the overall structure of the boundary layer above a coral reef canopy can be captured using simple geometric surrogates for coral heads. Consistent with Reidenbach *et al.* (2006), while skin drag is important for mass

https://doi.org/10.1017/jfm.2024.1179 Published online by Cambridge University Press

transfer rates and diffusion, it is form drag from larger-scale roughness that contributes most to overall canopy drag. Therefore, it may be practical to get estimates of drag from simplified geometries, especially when mean in-canopy and free-stream velocities are based on observed environmental conditions. The experimental results of this study suggest that exactly matching surface area and volume does not lead to significant changes in turbulence statistics or drag estimates. Instead, it is likely more imperative to replicate submergence ratio and canopy element spacing. However, because these results were obtained for a unidirectional flow only without waves, they should only be applied at high Keulegan–Carpenter numbers where drag, not inertia, dominates.

There are instances when it is likely more appropriate to use real coral heads instead of cylinders, specifically when the in-canopy dynamics is of primary importance. For example, small-scale topographical features play a larger role in mass transfer and diffusion rates which have been shown to be spatially dependent and peak at stagnation points (Chang *et al.* 2014). Additionally, studies show that larval transport and settlement is significantly affected by the local hydrodynamics (Crimaldi *et al.* 2002; Whitman & Reidenbach 2012). Coral larvae favour tightly spaced roughness with less shear (Reidenbach *et al.* 2021), so the cylinder's sharp edge and the defined wake could lead to inaccurate model results. Previous work by McDonald *et al.* (2006) suggests h_c/h plays a larger role in drag coefficient estimates in low Reynolds number flows, so using simplified roughness like cylinders may be less accurate in such cases.

Acknowledgements. We would like to thank the Stanford Oceans Department, and the Department of Civil and Environmental Engineering for their support of J.F.H., and the Bob and Norma Street Environmental Fluid Mechanics Laboratory, and Stanford's Office of the Vice Provost for Undergraduate Education Fellowship Program for their generous support of B.Z.K. We would also like to thank to C. Anderson and B. Sabala for their assistance with the experimental set-up and E. Boles for valuable discussions.

Declaration of interests. The authors report no conflict of interest.

Author ORCIDs.
J.F. Hamilton https://orcid.org/0009-0008-8392-9611;
S.G. Monismith https://orcid.org/0000-0002-7388-3313;
J.R. Koseff https://orcid.org/0000-0003-2121-4844.

References

Asher, S., Niewerth, S., Koll, K. & Shavit, U. 2016 Vertical variations of coral reef drag forces. *J. Geophys. Res.: Oceans* **121** (5), 3549–3563.

Asher, S. & Shavit, U. 2019 The effect of water depth and internal geometry on the turbulent flow inside a coral reef. *J. Geophys. Res.: Oceans* **124** (6), 3508–3522.

Atkinson, M.J. & Bilger, R.W. 1992 Effects of water velocity on phosphate uptake in coral reef-hat communities. *Limnol. Oceanogr.* **37** (2), 273–279.

Baldock, T.E., Shabani, B., Callaghan, D.P., Hu, Z. & Mumby, P.J. 2020 Two-dimensional modelling of wave dynamics and wave forces on fringing coral reefs. *Coast. Engng* **155**, 103594.

de Boor, C.R. 1980 A practical guide to splines. *Maths Comput.* **34** (149), 325–326.

Brunet, Y. 2020 Turbulent flow in plant canopies: historical perspective and overview. *Boundary-Layer Meteorol.* **177** (2–3), 315–364.

Burke, L., Reytar, K., Spalding, M. & Perry, A. 2011 Reefs at risk revisited. *Tech. Rep.* 3.

Chang, S., Iaccarino, G., Ham, F., Elkins, C. & Monismith, S. 2014 Local shear and mass transfer on individual coral colonies: computations in unidirectional and wave-driven flows. *J. Geophys. Res.: Oceans* **119** (4), 2599–2619.

Crimaldi, J.P., Thompson, J.K., Rosman, J.H., Lowe, R.J. & Koseff, J.R. 2002 Hydrodynamics of larval settlement: the influence of turbulent stress events at potential recruitment sites. *Limnol. Oceanogr.* **47** (4), 1137–1151.

Dimotakis, P.E. 2000 The mixing transition in turbulent flows. *J. Fluid Mech.* **409**, 69–98.

https://doi.org/10.1017/jfm.2024.1179 Published online by Cambridge University Press

GORING, D.G. & NIKORA, V.I. 2002 Despiking acoustic Doppler velocimeter data. *J. Hydraul. Engng ASCE* **128** (1), 117–126.

HEARN, C.J. 2011 Perspectives in coral reef hydrodynamics. *Coral Reefs* **30** (Suppl. 1), 1–9.

HENCH, J.L. & ROSMAN, J.H. 2013 Observations of spatial flow patterns at the coral colony scale on a shallow reef flat. *J. Geophys. Res.: Oceans* **118** (3), 1142–1156.

HOEGH-GULDBERG, O., *et al.* 2007 Coral reefs under rapid climate change and ocean acidification. *Science* **318**, 1737–1742.

LENTZ, S.J., DAVIS, K.A., CHURCHILL, J.H. & DECARLO, T.M. 2017 Coral reef drag coefficients – water depth dependence. *J. Phys. Oceanogr.* **47** (5), 1061–1075.

LIN, C.C. 1953 On Taylor's hypothesis and the acceleration terms in the Navier–Stokes equation. *Q. Appl. Maths* **10** (4), 295–306.

LINDHART, M., MONISMITH, S.G., KHRIZMAN, A., MUCCIARONE, D. & DUNBAR, R. 2021 How consistent are estimates of roughness parameters on a rough coral reef? *J. Geophys. Res.: Oceans* **126** (12).

LOWE, R.J., KOSEFF, J.R. & MONISMITH, S.G. 2005*a* Oscillatory flow through submerged canopies: 1. Velocity structure. *J. Geophys. Res.: Oceans* **110** (10), 1–17.

LOWE, R.J., KOSEFF, J.R., MONISMITH, S.G. & FALTER, J.L. 2005*b* Oscillatory flow through submerged canopies: 2. Canopy mass transfer. *J. Geophys. Res.: Oceans* **110** (10).

LOWE, R.J., SHAVIT, U., FALTER, J.L., KOSEFF, J.R. & MONISMITH, S.G. 2008 Modeling flow in coral communities with and without waves: a synthesis of porous media and canopy flow approaches. *Limnol. Oceanogr.* **53** (6), 2668–2680.

LUMLEY, J.L. 1965 Interpretation of time spectra measured in high-intensity shear flows. *Phys. Fluids* **8** (6), 1056–1062.

MADIN, J.S. 2005 Mechanical limitations of reef corals during hydrodynamic disturbances. *Coral Reefs* **24** (4), 630–635.

MADIN, J.S. & CONNOLLY, S.R. 2006 Ecological consequences of major hydrodynamic disturbances on coral reefs. *Nature* **444** (7118), 477–480.

MANDEL, T.L., ROSENZWEIG, I., CHUNG, H., OUELLETTE, N.T. & KOSEFF, J.R. 2017 Characterizing free-surface expressions of flow instabilities by tracking submerged features. *Exp. Fluids* **58** (11).

MCDONALD, C.B., KOSEFF, J.R. & MONISMITH, S.G. 2006 Effects of the depth to coral height ratio on drag coefficients for unidirectional flow over coral. *Limnol. Oceanogr.* **51** (3), 1294–1301.

MORI, N., SUZUKI, T. & KAKUNO, S. 2007 Noise of acoustic doppler velocimeter data in bubbly flows. *J. Engng Mech.* **133** (1), 122–125.

NEPF, H.M. & VIVONI, E.R. 2000 Flow structure in depth-limited, vegetated flow. *J. Geophys. Res.: Oceans* **105** (C12), 28547–28557.

O'RIORDAN, C.A., MONISMITH, S.G. & KOSEFF, J.R. 1993 A study of concentration boundary-layer formation over a bed of model bivalves. *Limnol. Oceanogr.* **38** (8), 1712–1729.

POMEROY, A.W.M., GHISALBERTI, M., PETERSON, M. & FAROOJI, V.E. 2023 A framework to quantify flow through coral reefs of varying coral cover and morphology. *PLoS ONE* **18** (1), e0279623.

POPE, S.B. 2012 *Turbulent Flows*. Cambridge University Press.

REIDENBACH, M.A., KOSEFF, J.R. & KOEHL, M.A.R. 2009 Hydrodynamic forces on larvae affect their settlement on coral reefs in turbulent, wavedriven flow. *Limnol. Oceanogr.* **54** (1), 318–330.

REIDENBACH, M.A., KOSEFF, J.R. & MONISMITH, S.G. 2007 Laboratory experiments of fine-scale mixing and mass transport within a coral canopy. *Phys. Fluids* **19** (7).

REIDENBACH, M.A., MONISMITH, S.G., KOSEFF, J.R., YAHEL, G. & GENIN, A. 2006 Boundary layer turbulence and flow structure over a fringing coral reef. *Limnol. Oceanogr.* **51** (5), 1956–1968.

REIDENBACH, M.A., STOCKING, J.B., SZCZYRBA, L. & WENDELKEN, C. 2021 Hydrodynamic interactions with coral topography and its impact on larval settlement. *Coral Reefs* **40** (2), 505–519.

ROGERS, J.S., MATICKA, S.A., CHIRAYATH, V., WOODSON, C.B., ALONSO, J.J. & MONISMITH, S.G. 2018 Connecting flow over complex terrain to hydrodynamic roughness on a coral reef. *J. Phys. Oceanogr.* **48** (7), 1567–1587.

ROSMAN, J.H. & HENCH, J.L. 2011 A framework for understanding drag parameterizations for coral reefs. *J. Geophys. Res.: Oceans* **116** (8), C08025.

SHAPIRO, O.H., FERNANDEZ, V.I., GARREN, M., GUASTO, J.S., DEBAILLON-VESQUE, F.P., KRAMARSKY-WINTER, E., VARDI, A. & STOCKER, R. 2014 Vortical ciliary flows actively enhance mass transport in reef corals. *Proc. Natl Acad. Sci. USA* **111** (37), 13391–13396.

STOCKING, J.B., LAFORSCH, C., SIGL, R. & REIDENBACH, M.A. 2018 The role of turbulent hydrodynamics and surface morphology on heat and mass transfer in corals. *J. R. Soc. Inter.* **15** (149).

https://doi.org/10.1017/jfm.2024.1179 Published online by Cambridge University Press

TAKESHITA, Y., MCGILLIS, W., BRIGGS, E.M., CARTER, A.L., DONHAM, E.M., MARTZ, T.R., PRICE, N.N. & SMITH, J.E. 2016 Assessment of net community production and calcification of a coral reef using a boundary layer approach. *J. Geophys. Res.: Oceans* **121** (8), 5655–5671.

WELLINGTON, G.M. 1982 An experimental analysis of the effects of light and zooplankton on coral zonation. *Oecologia* **52** (3), 311–320.

WHITMAN, E.R. & REIDENBACH, M.A. 2012 Benthic flow environments affect recruitment of Crassostrea virginica larvae to an intertidal oyster reef. *Mar. Ecol. Prog. Ser.* **463**, 177–191.

https://doi.org/10.1017/jfm.2024.1179 Published online by Cambridge University Press